Future reduction of cold extremes over East Asia due to thermodynamic and dynamic warming

Donghuan Li[1, 3], Tianjun Zhou[2, 3, 5*], Youcun Qi[1, 3], Liwei Zou[2], Chao Li[4], Wenxia Zhang[2], Xiaolong Chen[2]

[1]*Key Laboratory of Water Cycle and Related Land Surface Processes, Institute of Geographic Sciences and Natural Resources Research, Chinese Academy of Sciences, Beijing, China*

[2]*LASG, Institute of Atmospheric Physics, Chinese Academy of Science, Beijing, China*

[3]*University of Chinese Academy of Sciences, Beijing, China*

[4]*Max Planck Institute for Meteorology, Hamburg, Germany*

[5]*CAS Center for Excellence in Tibetan Plateau Earth Sciences, Chinese Academy of Sciences (CAS), Beijing, China*

Corresponding author:

Dr. Tianjun ZHOU

LASG, Institute of Atmospheric Physics

Chinese Academy of Sciences

Beijing 100029, China.

Phone: 86-10-8299-5279

Fax: 86-10-8299-5172

E-mail: *zhoutj@lasg.iap.ac.cn*

Abstract

Cold extremes have large impacts on human society. Understanding the physical processes dominating the changes of cold extremes is crucial for a reliable projection of future climate change. The observed cold extremes have ~~been~~ decreased during the last several decades and this trend will continue under ~~the~~ future global warming. Here, we quantitatively identify the contributions of dynamic (changes in large-scale atmospheric circulation) and thermodynamic (rising temperatures resulting from global warming) effects to East Asian cold extremes in the past several decades and in a future warm climate by using two sets of large ensemble ~~simulation~~simulations of climate models. We show that the dynamic component accounts for over 80% of the cold-month (coldest 5% boreal winter months) surface air temperature (SAT) anomaly in the past five decades. However, in a future warm climate, the thermodynamic change is the main contributor to the decreases in the intensity and occurrence probability of East Asian cold extremes, while the dynamic change is also contributive. The intensity of East Asian cold extremes will decrease by around 5°C at the end of the 21st century, in which the thermodynamic (dynamic) change contributes approximately 75% (25%). The present-day (1986-2005) East Asian cold extremes will almost never occur after around 2035, and this will happen eight years later due solely to thermodynamic change. The upward trend of a positive Arctic Oscillation-like sea level pressure pattern dominates the changes in the dynamic component. The finding provides a useful reference for policymakers in climate change adaptation activities.

~~**Key words**~~**Keywords:** East Asian cold extreme, dynamic adjustment, global warming

1 Introduction

Extreme events are widely ~~concerned~~concerning because of their high destructive power and great social impacts. Cold extremes have great impacts on agriculture, transportation, ~~,~~ and people's health, and can even cripple power supplies and ~~led~~lead to rolling blackouts (Steponkus, 1979; Andreescu and Frost, 1998; Sheridan et al., 2015; Thornton et al., 2016). The global mean surface air temperature (SAT) has been increasing in the past century due to the increase of anthropogenic greenhouse gas concentration in the atmosphere (Jones et al., 2008; IPCC, 2021). While warm extremes continue to attract considerable attention from the scientific community and ordinary people (e.g. Alexander et al., 2006; Rahimzadeh et al., 2009; Donat et al., 2012; Sun et al., 2014; Ma et al., 2017b), the cold extremes have also gained wide attention (e.g. Overland et al., 2011; Mori et al., 2014; Li et al., 2015; McCusker et al., 2016; Sun et al., 2016; Trenary et al., 2016; Ma et al., 2018; Qian et al., 2018) due to the mid-latitude cold extremes happened in recent several years.

A strong cold surge related to the negative phase of the Arctic Oscillation (AO) and intensified Siberian High attacked North China during 6-8 January 2021~~.~~ (Wang et al., 2021). The temperatures reached or broke the records in more than 50 cities and counties. Beijing experienced the third coldest day since 1951 on 7 January, with a daily minimum temperature of -19.6°C. (Wang et al., 2021; Zhou et al., 2022). ~~The~~The regional mean temperature in North China during 6-8 January 2021 was about 9°C lower than the average for the same period between the years 2001 and 2020. North America evidenced a widespread cold extreme in February 2021, which was caused by

the distorted and weakened polar vortex (Lee, 2021; Lu et al., 2021). The temperatures were 15°C to 25°C lower than normal in large areas and caused huge impacts on the energy supplies and transportation (Zhou et al., 2022). Cold ~~extreme occurs~~extremes have occurred from time to time under global warming in recent years. Will it continue to occur ~~if the~~while global warming continues in the future?

The model simulations indicate that the anthropogenic influences have reduced the occurrence probability of cold extremes over eastern China with intensity stronger than the record-breaking cold extreme ~~in~~(since modern meteorological observations started in 1960) on 21-25 January 2016 (Qian et al., 2018). The wintertime East Asian SAT is projected to increase significantly as a response to ~~the~~ future global warming (IPCC, 2021). Cold months defined based on the 20th century will be rarer under ~~the~~ future global warming (Räisänen and Ylhäisi, 2011) and the future warming will continuously reduce the intensity and occurrence probability of the cold extreme events (annual minimum daily minimum temperature) over East Asia (Kharin et al., 2013; 2018).

Previous studies demonstrated that the SAT is influenced by both the dynamic (changes in large-scale atmospheric circulation) and thermodynamic effects (Thompson et al., 2009; Cattiaux et al., 2010; Wallace et al., 2012; Smoliak et al., 2015; Deser et al., 2016). The dynamic effect, for example, the Arctic amplification, which reduces the polar-to-equator temperature gradient, can further modify the atmospheric circulation. There is a positive AO-like SLP (sea level pressure) changing pattern under ~~the~~ global warming (Fyfe et al., 1999; Yamaguchi and Noda, 2006; Kitoh, 2017) and

the East Asian winter monsoon will be weakened in the warmer future conditions according to the multi-model simulations of the CMIP3 and CMIP5 models (Jiang and Tian, 2013; Xu et al., 2016). However, there is a lack of quantitative research on the contributions of the dynamic and thermodynamic effects to the future changes of the East Asian cold extremes if the global mean SAT continues to increase.

The "dynamic adjustment" ~~approaches~~approach (Wallace et al., 2012; Smoliak et al., 2015; Deser et al., 2016) ~~have~~has been proposed to divide the SAT anomaly into dynamic component (solely associated with circulation changes) and thermodynamic component (associated with thermodynamic processes). The dynamic adjustment of the North Hemisphere SAT field based on SLP can be used to investigate both the short-term climate fluctuations and long-term trends of SAT (Smoliak et al., 2015). Deser et al. (2016) indicates that the internal circulation trends ~~accounts~~account for over 30% of the North American wintertime warming trend in the past 50 years. The variability of circulation plays a critical role in the evolution of the East Asian winter temperature trends during 1961-2018 and the internally induced dynamic component offsets the forced warming by over 70% in northern East Asia over the time period of 1979–2018 (Gong et al., 2019; 2021). The dynamic adjustment approach has also been used to investigate the wintertime precipitation changes and summertime SAT changes over East Asia (e.g., Guo et al., 2019; Hu et al., 2019). However, these studies mainly focus on the mean temperature and mean precipitation changes in the past several decades, ~~our knowledge on~~very few studies have quantified the contributions of the dynamic and thermodynamic effects to the future changes of the East Asian cold extremes associated

with global warming ~~remains quite limited~~.

By using two sets of grand ensemble simulations combined with observational data and reanalysis data, we aim to answer the following questions: (1) What are the relative contributions of the dynamic and thermodynamic effects to the East Asian cold extremes in the past several decades? (2) How will the intensity and occurrence probability of East Asian cold extremes change in the warmer future~~? (3) What~~ and what are the quantitative contributions of the dynamic and thermodynamic effects to the changes of East Asian cold extremes in the warmer future? (3) How will the circulation change in the warmer future and how will this change affect cold extremes in East Asia?

2 Data and Methodology

2.1. Model Data

The 100-member Grand Ensemble generated by the Max Planck Institute Earth System Model version 1.1 (MPI-GE; Maher et al., 2019) with horizontal resolution of 1.8°×1.8° and the 40-member Community Earth System Model Large Ensemble (CESM-LE; Kay et al., 2015) with horizontal resolution of 1°×1° are applied in this study to investigate the contributions of dynamic and thermodynamic components to the East Asian cold extremes in recent decades and the future warm climate. The historical simulations integrated from 1850 to 2005 in the MPI-GE and from 1920 to 2005 in the CESM-LE were driven by the observed forcings. The Representative Concentration Pathway 8.5 (RCP8.5) scenario simulations were performed from 2006

to 2099 in the MPI-GE and from 2006 to 2100 in the CESM-LE. In addition, the 2000-yr MPI pre-industrial (PiCTL) simulation and 1800-yr CESM PiCTL simulation are also used in this study. For more detailed information ~~of~~on the MPI-GE and the CESM-LE, please refer to Maher et al. (2019) and Kay et al. (2015), respectively.

2.2 Observation Data

The following datasets are used in this study: (1) monthly mean SAT from the Climatic Research Unit (CRU) version 4 with a horizontal resolution of 0.5°×0.5° (Harris et al., 2014). (2) Monthly mean three-dimensional circulation fields derived from the 20th Century Reanalysis (20CR) version 2 with a horizontal resolution of 2°×2° (Compo et al., 2011). The time period for these two datasets used in this study is from 1920 to 2012.

2.3 Dynamic Adjustment Approach

The dynamic adjustment method presented by Deser et al. (2016) is based on the constructed circulation analogue using SLP. This method empirically divides SAT variability into a dynamic component (associated with atmospheric circulation changes) and a thermodynamic component (the residual part). The dynamic adjustment method is summarized below and please refer to Deser et al. (2016) for more details.

2.3.1 Application to the MPI-GE and CESM-LE

For a given "target" month and year (e.g. December 1990) in each ensemble member, we rank the 2000 (1800) December SLP fields in the PiCTL simulation by their similarity with the target SLP pattern according to Euclidean distance. ~~Then, we~~

~~randomly select 100 SLP fields from~~From the 150 ~~closest~~ SLP fields with the smallest Euclidean ~~distance~~ distances, we randomly subsample 100 SLP fields to construct ~~a~~the best estimation of the target SLP pattern by linear combination. The same set of linear coefficients is applied to the accompanying SAT fields~~. We repeat the above procedure for 100 times and average the 100 linear combinations to derive the dynamically induced SAT field in the target month.~~ to obtain the associated linear combination of SAT. We repeat the subsampling procedure 100 times and average the 100 linear combinations to derive the dynamically induced SAT field in the target month. Deser et al. (2016) illustrate the importance of this iterative random selection process and the reason for the repeated subsampling procedure is to take into account the uncertainty related to internal thermodynamic variability and to ensure the robustness of the results. We use the domain 15°~90°N, 30°~180°E for the SLP analogues. The sensitivity to the precise region used is small (Figures not shown; e.g. within ±5° of latitude and ±10° of longitude). To test whether 150 selected SLP fields are sufficient to estimate the target SLP, a sensitivity analysis is conducted on the sample size of the selected closest fields. The findings suggest that there is no significant difference when the number of selected fields exceeds 100.

The multi-member mean of the dynamic component is regarded as the forced dynamic component and the internal dynamic component is obtained by subtracting the forced part from the total dynamic component~~.~~ for each ensemble member. Thermodynamic components are obtained as residuals (total minus dynamic) for both forced and internal components.

2.3.2 Application to the observation

There is no PiCTL simulation in the observation. Therefore, before computing the dynamic component of SAT, the quadratic trend of the SAT during 1920-2012 is first subtracted to obtain SAT series without anthropogenic forcing. ~~For a given~~Similar to the application to the model ensembles, for each month and year in the observation, 40 SLP fields subsampled from 60 closest SLP fields are first selected (excluding the target month). ~~Dynamic~~Then, dynamic adjustment procedure described in section 3.2.1 is ~~then~~ applied to derive the dynamically-induced SAT fields in the observation.

Different from model simulations, there is only one member in the observation, we cannot separate the forced and internal parts by calculating the ensemble mean or subtracting the ensemble mean. To obtain the internal dynamic contribution to the observed SAT anomaly, a separate dynamic adjustment based on the internal component of the observed SLP anomalies is performed. ~~The~~It is worth noting that, the internal component of the observed SLP anomalies is obtained by subtracting the model ensemble-mean SLP anomaly from the observed SLP anomaly at each time step. ~~Then~~

After we get the internal dynamic component of SAT anomaly, the forced dynamic component is calculated by subtracting the internal dynamic component from the total dynamic component. Thermodynamic components are obtained as residuals (total minus dynamic) for both forced and internal components.

2.4 Baseline period and the study region

The baseline period of 1986-2005 boreal winter is referred to as the historical

(present-day) climatology to investigate the SAT anomalies and contributions of dynamic and thermodynamic effects to future changes of East Asian cold extremes. The certain region (the black box in Figure 2) from 20°N to 55°N and from 105°E to 130°E is regarded as East Asia in this study.

2.5 The definitions of cold extreme and cold month

The definition of East Asian cold extreme is as follows: in the models, the regional averaged monthly SAT anomaly of East Asia is firstly calculated. ~~Then~~For a specific period, cold extremes are defined as the months in which the regional mean SAT is lower than the statistical 5th percentile of the climatological monthly SAT series during DJF in ~~a certain~~this time ~~slice~~period. A month when a cold extreme happens is defined as a cold month. Similarly, the cold months in the observation are the 8 coldest months (5% of 150 winter months) during the 1962-2011 boreal winter (Table 1).

All the anomalies shown in this study are calculated relative to the climatological values of the 1986-2005 boreal winter unless mentioned otherwise. Student's t--test is applied to indicate the 5% significance level.

2.6 The intensity and occurrence probability ratio of cold extreme

The intensity of a cold extreme is the SAT deviation relative to the present-day boreal winter SAT climatology.

The occurrence probability ratio of the present-day cold extremes is calculated as follows (Ma et al., 2017a):

$$\mathrm{PR} = \frac{P1}{P0} \quad (1)$$

where PR is the occurrence probability ratio. The value of $P0$ is 5%, and $P1$ is the probability of monthly SAT lower than the present-day cold extreme threshold in other time periods. For example, if the value of $P1$ is 2% during a future period, then the value of PR is 0.4. For the calculation of the occurrence probability ratio, we pull all the members together ~~ratio~~ rather than calculate it for each member.

3 Results

3.1 Dynamic and thermodynamic processes to East Asian cold extremes in recent decades

The observed winter temperature in East Asia shows obvious variability during the 1962-2011 boreal winter~~,~~ (Figure 1a). According to the correlation coefficients calculated between each component of the SAT anomaly and ~~this~~the original SAT anomaly, the SAT variability is mainly caused by the dynamically~~-~~ induced internal component~~. Moreover, this~~ (Figure 1b-g). The fluctuations of forced dynamic and thermodynamic components are much smaller than those of internal dynamic and thermodynamic ones (Figure 1c, d, f and g). Internal variability is the main cause of cold extremes over East Asia in the past five decades (Figure 1).

The decomposition of the observed East Asian cold-month SAT anomalies during the 1962-2011 boreal winter is shown in Figure 2a-c. The SAT is significantly lower than the present-day winter SAT climatology (more than 3℃) across the East Asian landmass (Figure 2a). The decomposition of the SAT anomaly indicates that the cold

extremes in recent decades are mainly caused by the dynamic component (Figure 2b and c~~), especially for the cold extremes happened in recent years. For example, the~~). The dynamic component accounts for approximately 55% of the total East Asian cold-month SAT anomaly during the 1962-2011 boreal winter. Compared to cold extremes in the 1960s and 1970s, the percentage contribution of dynamic components to the cold extreme in January 2011 is higher (Table 1). The East Asian regional mean SAT anomaly in January 2011 is -3.47℃, in which, the dynamic component is -3.81℃, accounting for up to 110% of the total SAT anomaly (Table 1). It is worth noting that these cold extremes are mainly caused by the internally- generated components, and the forced dynamic component ~~shows~~has shown little trend in the past five decades and has little contribution to the observed cold extremes (Figure 1c and d).

The two sets of large ensemble model simulations can ~~well reproduce~~generally capture the ~~relative contributions~~spatial distributions of total SAT anomaly and the dynamic ~~and thermodynamic components to the~~component of cold extremes during 1962-2011 boreal winter (Figure 2d~~ i). The SAT is significantly lower~~, e, g and h), with pattern correlation coefficients higher than ~~the winter SAT climatology throughout~~ 0.7 in both model ensembles. However, the thermodynamic component is much weaker in the model simulations than in the observation, especially in the northern parts of East Asia (Figure ~~2d and g)~~2f and ~~the~~i). The dynamic component is the main contributor to the cold extremes ~~(Figure 2e, f, h and i). It should be noted that there are much more cold extreme samples in the MPI-GE and the CESM-LE, and the contribution of the dynamic component to the cold extremes are more evident in the two model ensembles~~

~~than in the observation (Figure 2). The dynamic component accounts~~, accounting for up to 85% and 82% of the total East Asian cold-month SAT anomaly during the 1962-2011 boreal winter in the MPI-GE and the CESM-LE, respectively. Compared with the observation, the contribution of the dynamic component to the cold extremes is larger in the two model ensembles (Figure 2). One possible reason is that there are only 8 cold extreme samples in the observation, and the relative contributions of dynamic and thermodynamic components cannot be fully reflected by these samples. Another possible reason may be the uncertainty of local thermodynamic processes (Röthlisberger and Papritz, 2023).

The results shown above indicate that the observed cold extremes in the past decades are mainly caused by the internal variability of atmospheric circulations. The cold extremes are often associated with strong East Asian winter monsoon flows, which are often accompanied ~~with~~by the blockings in the Urals and the intensified Siberian high~~.~~ (Francis and Vavrus, 2012; Ma et al., 2018). The composite circulation anomalies in the cold months during the 1962-2011 boreal winter are further investigated (Figure 3). A ridge-trough pattern is seen over the Eurasian continent in the upper troposphere and there is southeastward propagation of wave activity flux (Figure 3a). The westerlies are weakened in the whole troposphere around 45°N -75°N, and there is an enhanced meandering flow pattern (Figure 3b~~).~~; Walsh, 2014; Simmonds, 2015; Ma et al., 2018). The weakened westerlies may favor the blocking events, which have a strong relationship with the cold extremes over East Asia~~.~~ (Luo et al., 2017). The surface Siberian High is intensified, and low-level northerly winds lead cold Arctic air to spread

281 southward to East Asia (Figure 3c).

282 This typical type of circulation anomalies in cold months mentioned above are
283 also well captured in the MPI-GE and the CESM-LE (Figure 3d-f). Namely, there is a
284 ridge-trough pattern in the upper troposphere over the Eurasian continent and the
285 surface Siberian High is enhanced. The westerlies are weakened in the whole
286 troposphere and the cold air from the Arctic regions causes cold extremes over East
287 Asia.

288 **3.2 Dynamic and thermodynamic contributions to the projected changes in East**
289 **Asian cold extremes**

290 In the observations, the dynamic component is the main contributor to the East
291 Asian cold extremes in the past five decades. The human--induced global warming
292 ~~has~~had little ~~effects~~effect on the changes in dynamically-induced SAT anomalies during
293 1962-2011 (Figure 1). How will the dynamic and thermodynamic effects contribute to
294 the future changes in cold extremes over East Asia?

295 We first examine the changes in the intensity of East Asian cold extremes (Figure
296 4a and c). The SAT anomaly will continuously increase along with ~~the~~ global warming
297 under the RCP8.5 scenario. Compared with the present day, the East Asian regional
298 mean cold-month SAT will increase by approximately 4.8℃ at the end of the 21st
299 century according to the best estimation of MPI-GE (Figure 4a). The large center
300 ~~locates~~is located in Northeast China, over 6℃ (Figure 5a). The dynamic and
301 thermodynamic components will also continually increase under the RCP8.5 scenario.

It is worth noting that, the dynamic component explains a larger part of the total SAT anomaly in cold months before approximately 2040. Thereafter, the thermodynamic component is the main driver in both model ensembles (Figure 4a and c). The increases in the dynamic and thermodynamic components are approximately 1.3℃ and 3.5℃ at the end of the 21st century, respectively, in the MPI-GE (Figure 4a). Therefore, the contribution of the increase in dynamic component to the total SAT increase is 27%. The dynamic and thermodynamic components also increase faster in northern parts of East Asia than in other regions (Figure 5b and c). The faster increase of thermodynamic ~~components~~component in northern East Asia may be caused by the snow-albedo feedback~~,~~ (Fischer et al., 2011), while the reason for the faster increase in dynamic component in this region is that the influence of East Asian Winter Monsoon on northern East Asia is more evident than on other subregions~~.~~ (He et al., 2017). The results in the CESM-LE are generally consistent with those in the MPI-GE. The East Asian regional mean SAT anomalies in cold months will increase by approximately 5.2℃ at the end of the 21st century (Figure 4c). The corresponding increases in the dynamic and thermodynamic components are 1.3℃ and 3.9℃, respectively. Statistically, the contribution of the increase in dynamic component to the total SAT increase is about 25%. From the perspective of spatial distribution, ~~the~~ total SAT and its dynamic and thermodynamic components show similar changing patterns ~~of the total SAT and the dynamic component are similar~~ in the two sets of large ensemble model simulations, with large increases occurring in northern parts of East Asia (Figure ~~5a, b, d and e). The~~ 5). However, there are some local differences between the two models. Compared with

MPI-GE, the end-of-the 21st-century increase in cold-month regional mean SAT is approximately 0.4℃ higher in CESM-LE, primarily due to the thermodynamic component ~~shows some differences (Figure 5c~~. The larger increase of thermodynamic component in Northeast and ~~f~~Southeast China in CESM-LE than in MPI-GE may be attributed to differences in thermal feedback processes, such as the snow-albedo feedback and land-surface fluxes (Seneviratne et al., 2010; Fischer et al., 2011; Röthlisberger and Papritz, 2023).

We extend the analysis from the changes in the intensity of cold extremes to the changes in the occurrence probability ratio of the present-day cold extremes in the future warm climate (Figure 4b). The 20-year running occurrence probability ratio of the present-day cold extremes will rapidly decrease under the RCP8.5 scenario in both sets of the large ensemble model simulations. In the MPI-GE, the occurrence probability ratio of the present-day cold extremes will decrease to 0.05 in the period from 2034 to 2053 (Figure 4b), which means the present-day cold extremes will almost never occur after 2034. We isolate the dynamic and thermodynamic contributions to the changes ~~of~~in the occurrence probability ratio of the present-day cold extremes. If we hold the dynamic component constant at the present-day level, and allow the thermodynamic component to evolve according to the model projection, the year when the occurrence probability ratio of the present-day cold extremes will decrease to 0.05 is 2042, eight years later than the time mentioned above (Figure 4b). Correspondingly, if we hold the thermodynamic component constant at the present-day level, and allow the dynamic component to evolve according to the model projection, the occurrence

probability ratio of the present-day cold extremes will decrease to 0.2 at the end of the 21st century. From the perspective of spatial distribution, the occurrence probability ratio of the present-day cold extremes will be decreased to 0.05 before 2040 in parts of southeastern China, northeastern China and the Korean Peninsula (Figure 6a). The results in the CESM-LE are generally consistent with those in the MPI-GE (Figures 4d and 6b). The occurrence probability ratio of the present-day cold extremes will decrease to 0.05 in 2035-2054 (Figure 4d) and the occurrence probability ratio also decreases faster in southeastern China, parts of northeastern China and the southern Korean Peninsula (Figure 6b). Different from the MPI-GE, the occurrence probability ratio of the present-day cold extremes will decrease to 0.05 after 2060 in parts of North China ~~and Northeast China~~ in the CESM-LE (Figure 6b).

The thermodynamic ~~change is~~component dominates the ~~main contributor to the decreases~~future decrease in the intensity and occurrence probability of East Asian cold extremes, while the dynamic ~~change~~component is also contributive. Dynamic change accounts for approximately one-quarter of the total change in the intensity of cold extremes by the end of the 21st century. We further examine the changes in SLP anomalies associated with East Asian cold extremes (Figures 7 and 8).

Similar to the previous studies (Fyfe et al., 1999; Cai et al., 2017; Kitoh, 2017), the projected changes in SLP exhibit a positive AO-like pattern, ~~particularly in the MPI-GE (Figure 7a and b).~~especially in MPI-GE (Figure 7). The pattern correlation coefficients between the SLP changing patterns and the positive phase of AO in MPI-GE and CESM-LE are approximately 0.7 and 0.4, respectively (Figure 7a and c). The

winter-mean SLP will be reduced in the Arctic regions and enhanced in the mid-latitude regions. The AO shows a highly positive correlation with the winter SAT anomaly over East Asia, especially the northern part, and the positive phase of AO is favorable for warm winter over East Asia (Gong et al., 2019; Wang et al., 2019). ~~Similar~~The SLP changing ~~pattern also occurs~~patterns in cold months (Figure ~~7c~~7b and d) are similar to those in winter mean (Figure 7a and c), and this is possibly the reason for the positive contribution of dynamic effects to the increase in SAT anomaly in cold months. We also construct the changes in the dynamic component of SLP (Figure 8). Changes in the dynamic component of SLP ~~corroborates~~also corroborate that the circulation changes are not favorable for the occurrence of East Asian cold extremes ~~(Figure 8c and d).~~ . There are some differences in the SLP changing patterns between the two model ensembles, particularly during cold extremes over the Eurasian region. This could be one of the possible reasons for the differences in local dynamic changes in the two model ensembles.

4 Summary and Discussion

4.1 Summary

Based on the dynamic adjustment approach, we utilized two sets of large ensemble model simulations in the MPI-GE and CESM-LE to investigate the contributions of the background warming (thermodynamic effect) and circulation changes (dynamic effect) to the East Asian cold extremes. The contributions of the two components to the East Asian cold extremes are quantitatively evaluated in the recent decades and under ~~the~~

future warming. The main conclusions are summarized as follows.

(1) The observed cold extremes in the past decades are mainly caused by the internal variability of atmospheric circulations~~, especially for the~~. Compared to cold extremes ~~happened~~in the 1960s and 1970s, the percentage contribution of dynamic component to the cold extreme in recent years is higher. Both MPI-GE and the CESM-LE are consistent in revealing the typical circulation anomalies associated with the East Asian cold extremes. ~~The relative contributions~~Compared with the observation, the contribution of the dynamic ~~and thermodynamic components~~component to the cold extremes ~~are well captured~~is more evident in the two model ensembles, and the dynamic component accounts for more than 80% of the total cold-month SAT anomalies in the past five decades.

(2) In the future warm climate, the ~~background warming is the main contributor to the~~ decreases in the intensity and occurrence probability of East Asian cold extremes are dominated by thermodynamic component, while the ~~circulation changes are~~ dynamic component is also contributive. ~~Compared~~According to MPI-GE and CESM-LE, compared with the present day, the mean intensity of the East Asian cold extremes will decrease by approximately 5°C at the end of the 21st century under the RCP8.5 scenario and the dynamic component contributes to a quarter of this decrease. The occurrence probability ratio of the present-day cold extremes will almost never occur after around 2035, and if we hold the dynamic component constant at the present-day level, this will happen approximately 8 years later.

(3) Positive AO-like sea level pressure pattern upward trend is projected in both of the model ensembles, ~~though there are a few differences between the two ensemble projection, and this change in large-scale circulation~~which is unfavorable to the occurrence of East Asian cold extremes. There are a few differences between the two ensemble projections, particularly in the Eurasian region during cold extremes, and this could be one of the possible reasons for the local differences of dynamic components in the two model ensembles.

4.2 Discussion

Substantial efforts have been devoted so far to ~~understand~~understanding the response of climate extremes to global warming (e.g. Alexander et al., 2006; Sanderson et al., 2017; Zhang et al., 2018; AghaKouchak et al., 2020; Li et al., 2021), as well as their physical mechanisms (Cattiaux et al., 2010; Peing and Magnusdottir~~–~~, 2014; Westra et al., 2014; Boschat et al., 2015; Horton et al., 2015; Qian et al., 2018). In particular, the thermodynamic processes (i.e., direct results of global warming) of changes in climate extremes have been well demonstrated. However, it remains ambiguous regarding how the dynamic processes will change under global warming, which is an important source of projection uncertainty for climate extremes (Shepherd, 2014; Norris et al., 2019). Hence, it is of vital importance to understand the dynamic changes of climate extremes, in order to improve the reliability of extreme climate projections.

In this study, we used two sets of large ensemble ~~simulations~~simulation data and

a dynamic adjust method to investigate the future change of cold extremes in East Asia, with a focus on understanding the thermodynamic and dynamic processes. Our results consistently show that the thermodynamic process is the dominant factor of future changes in East Asian cold extreme, with the contribution of dynamic process accounting for approximately one-quarter of the total change. In addition, the change in the dynamic component is attributed to the upward trend of a positive AO-like sea level pressure pattern, and this has been supported by previous studies (Fyfe et al., 1999; Cai et al, 2017; Kitoh, 2017).

AO is the main circulation mode in the non-tropical regions of the Northern Hemisphere in winter (Thompson and Wallace, 1998), and has a significant impact on the winter climate in East Asia (Gong et al., 2001). However, it is worth noting that future winter temperature changes in East Asia may also be impacted by other large-scale circulation factors (Zhou et al., 2007; Cheung et al., 2012; He and Wang, 2013). The quantitative impacts of potential future changes of different circulation factors on cold extremes in East Asia remain unclear and require further investigation in future research.

Data availability

The MPI-GE experiment products can be downloaded from https://esgf-data.dkrz.de/search/mpi-ge/. The specific experiments or variables can be selected through the navigation bar on the left-hand side. The monthly sea level pressure (psl), surface air temperature (tas), three-dimensional wind field (ua, va, wap), and geopotential height (zg) from the piControl, historical and rcp85 experiments are used in this work.

The CESM-LE experiment products can be downloaded from https://www.earthsystemgrid.org/dataset/ucar.cgd.ccsm4.cesmLE.html.

Author contribution

TJZ designed the study. DHL performed the data analysis, produced the figures and wrote the manuscript draft. YCQ and CL collected the datasets. LWZ, WXZ and XLC contributed to the analysis methods. All the authors contributed to the discussion, writing, and editing of the manuscript.

Competing interests

The authors declare that they have no conflict of interest.

~~Acknowledgments~~

Acknowledgements

This work is jointly supported by the National Natural Science Foundation of China (Grant Nos. 42105031, 41988101).

References

AghaKouchak, A., Chiang, F., Huning, L. S., Love, C. A., Mallakpour, I., Mazdiyasni, O., ... & Sadegh, M. (2020). Climate extremes and compound hazards in a warming world. Annual Review of Earth and Planetary Sciences, 48, 519-548. https://doi.org/10.1146/annurev-earth-071719- 055228.

Alexander, L. V., Zhang, X., Peterson, T. C., Caesar, J., Gleason, B., Klein Tank, A. M. G., ... & Vazquez‐Aguirre, J. L. (2006). Global observed changes in daily climate extremes of temperature and precipitation. Journal of Geophysical Research: Atmospheres, 111(D5). https://doi.org/10.1029/2005JD006290

Andreescu, M. P., & Frost, D. B. (1998). Weather and traffic accidents in Montreal, Canada. Climate research, 9(3), 225-230. https://doi.org/10.3354/cr009225

Boschat, G., Pezza, A., Simmonds, I., Perkins, S., Cowan, T., & Purich, A. (2015). Large scale and sub-regional connections in the lead up to summer heat wave and extreme rainfall events in eastern Australia. Climate Dynamics, 44, 1823-1840. https://doi.org/10.1007/s00382-014-2214-5.

Cai, W., Li, K., Liao, H., Wang, H., & Wu, L. (2017). Weather conditions conducive to Beijing severe haze more frequent under climate change. Nature Climate Change, 7(4), 257-262. https://doi.org/10.1038/nclimate3249

Cattiaux, J., Vautard, R., Cassou, C., Yiou, P., Masson‐Delmotte, V., & Codron, F. (2010). Winter 2010 in Europe: A cold extreme in a warming climate. Geophysical Research Letters, 37(20). https://doi.org/10.1029/2010GL044613

Cheung, H. N., Zhou, W., Mok, H. Y., & Wu, M. C. (2012). Relationship between Ural–Siberian blocking and the East Asian winter monsoon in relation to the Arctic Oscillation and the El Niño–Southern Oscillation. Journal of Climate, 25(12), 4242-4257. https://doi.org/10.1175/JCLI-D-11-00225.1

Compo, G. P., Whitaker, J. S., Sardeshmukh, P. D., Matsui, N., Allan, R. J., Yin, X., ... & Worley, S. J. (2011). The twentieth century reanalysis project. Quarterly Journal of the Royal Meteorological Society, 137(654), 1-28. https://doi.org/10.1002/qj.776

Deser, C., Terray, L., & Phillips, A. S. (2016). Forced and internal components of winter air temperature trends over North America during the past 50 years: Mechanisms and implications. Journal of Climate, 29(6), 2237-2258. https://doi.org/10.1175/JCLI-D-15-0304.1

Donat, M. G., & Alexander, L. V. (2012). The shifting probability distribution of global daytime and night‐time temperatures. Geophysical Research Letters, 39(14). https://doi.org/10.1029/2012GL052459

Fischer, E. M., Lawrence, D. M., & Sanderson, B. M. (2011). Quantifying uncertainties in projections of extremes—A perturbed land surface parameter experiment. Climate Dynamics, 37, 1381-1398.

Francis, J. A., & Vavrus, S. J. (2012). Evidence linking Arctic amplification to extreme weather in mid‐latitudes. Geophysical research letters, 39(6).

512 Fyfe, J. C., Boer, G. J., & Flato, G. M. (1999). The Arctic and Antarctic Oscillations
513 and their projected changes under global warming. Geophysical Research Letters,
514 26(11), 1601-1604. https://doi.org/10.1029/1999GL900317
515 Gong, D. Y., Wang, S. W., & Zhu, J. H. (2001). East Asian winter monsoon and Arctic
516 oscillation. Geophysical Research Letters, 28(10), 2073-2076.
517 https://doi.org/10.1029/2000GL012311
518 Gong, H., Wang, L., Chen, W., & Wu, R. (2019). Attribution of the East Asian winter
519 temperature trends during 1979–2018: Role of external forcing and internal
520 variability. Geophysical Research Letters, 46(19), 10874-10881.
521 https://doi.org/10.1029/2019GL084154
522 Gong, H., Wang, L., Chen, W., & Wu, R. (2021). Evolution of the East Asian winter
523 land temperature trends during 1961–2018: role of internal variability and external
524 forcing. Environmental Research Letters, 16(2), 024015. doi: 10.1088/1748-
525 9326/abd586
526 Guo, R., Deser, C., Terray, L., & Lehner, F. (2019). Human influence on winter
527 precipitation trends (1921–2015) over North America and Eurasia revealed by
528 dynamical adjustment. Geophysical Research Letters, 46(6), 3426-3434.
529 https://doi.org/10.1029/2018GL081316
530 Haarsma, R. J., Selten, F., Hurk, B. V., Hazeleger, W., & Wang, X. (2009). Drier
531 Mediterranean soils due to greenhouse warming bring easterly winds over
532 summertime central Europe. Geophysical research letters, 36(4).
533 https://doi.org/10.1029/2008GL036617

Harris, I. P. D. J., Jones, P. D., Osborn, T. J., & Lister, D. H. (2014). Updated high - resolution grids of monthly climatic observations–the CRU TS3. 10 Dataset. International journal of climatology, 34(3), 623-642. https://doi.org/10.1002/joc.3711

He, S., & Wang, H. (2013). Oscillating relationship between the East Asian winter monsoon and ENSO. Journal of Climate, 26(24), 9819-9838. https://doi.org/10.1175/JCLI-D-13-00174.1

He, S., Gao, Y., Li, F., Wang, H., & He, Y. (2017). Impact of Arctic Oscillation on the East Asian climate: A review. Earth-Science Reviews, 164, 48-62.

Horton, D. E., Johnson, N. C., Singh, D., Swain, D. L., Rajaratnam, B., & Diffenbaugh, N. S. (2015). Contribution of changes in atmospheric circulation patterns to extreme temperature trends. Nature, 522(7557), 465-469. https://doi.org/10.1038/nature14550

Hu, K., Huang, G., & Xie, S. P. (2019). Assessing the internal variability in multi-decadal trends of summer surface air temperature over East Asia with a large ensemble of GCM simulations. Climate Dynamics, 52(9), 6229-6242. https://doi.org/10.1007/s00382-018-4503-x

IPCC. (2021). Climate Change 2021. The Physical Science Basis. Contribution of Working Group I to the Sixth Assessment Report of the Intergovernmental Panel on Climate Change [Masson-Delmotte, V., P. Zhai, A. Pirani, S.L. Connors, C. Péan, S. Berger, N. Caud, Y. Chen, L. Goldfarb, M.I. Gomis, M. Huang, K. Leitzell, E. Lonnoy, J.B.R. Matthews, T.K. Maycock, T. Waterfield, O. Yelekçi, R. Yu, and

B. Zhou (eds.)]. Cambridge University Press, Cambridge, United Kingdom and New York, NY, USA, 2391 pp. doi:10.1017/9781009157896.

Jiang, D., & Tian, Z. (2013). East Asian monsoon change for the 21st century: Results of CMIP3 and CMIP5 models. Chinese Science Bulletin, 58(12), 1427-1435. https://doi.org/10.1007/s11434-012-5533-0

Jones, G. S., Stott, P. A., & Christidis, N. (2008). Human contribution to rapidly increasing frequency of very warm Northern Hemisphere summers. Journal of Geophysical Research: Atmospheres, 113(D2). https://doi.org/10.1029/2007JD008914

Kay, J. E., Deser, C., Phillips, A., Mai, A., Hannay, C., Strand, G., ... & Vertenstein, M. (2015). The Community Earth System Model (CESM) large ensemble project: A community resource for studying climate change in the presence of internal climate variability. Bulletin of the American Meteorological Society, 96(8), 1333-1349. https://doi.org/10.1175/BAMS-D-13-00255.1

Kharin, V. V., Flato, G. M., Zhang, X., Gillett, N. P., Zwiers, F., & Anderson, K. J. (2018). Risks from climate extremes change differently from 1.5 C to 2.0 C depending on rarity. Earth's Future, 6(5), 704-715. https://doi.org/10.1002/2018EF000813

Kharin, V. V., Zwiers, F. W., Zhang, X., & Wehner, M. (2013). Changes in temperature and precipitation extremes in the CMIP5 ensemble. Climatic change, 119(2), 345-357. https://doi.org/10.1007/s10584-013-0705-8

577 Kitoh, A. (2017). The Asian Monsoon and its Future Change in Climate Models: A
578 Review. Journal of the Meteorological Society of Japan, 95(1): 7-33.
579 https://doi.org/10.2151/jmsj.2017-002
580 Lee, S. H. (2021). The January 2021 sudden stratospheric warming. Weather, 76(4),
581 135-136. https://doi.org/10.1002/wea.3966
582 Li, C., Stevens, B., & Marotzke, J. (2015). Eurasian winter cooling in the warming
583 hiatus of 1998–2012. Geophysical Research Letters, 42(19), 8131-8139.
584 https://doi.org/10.1002/2015GL065327
585 Li, C., Zwiers, F., Zhang, X., Li, G., Sun, Y., & Wehner, M. (2021). Changes in annual
586 extremes of daily temperature and precipitation in CMIP6 models. Journal of
587 Climate, 34(9), 3441-3460. https://doi.org/10.1175/JCLI-D-19-1013.1
588 Lu, Q., Rao, J., Liang, Z., Guo, D., Luo, J., Liu, S., ... & Wang, T. (2021). The sudden
589 stratospheric warming in January 2021. Environmental Research Letters, 16(8),
590 084029. doi: 10.1088/1748-9326/ac12f4
591 Luo, D., Yao, Y., Dai, A., Simmonds, I., & Zhong, L. (2017). Increased quasi
592 stationarity and persistence of winter Ural blocking and Eurasian extreme cold
593 events in response to Arctic warming. Part II: A theoretical explanation. Journal of
594 Climate, 30(10), 3569-3587.
595 Ma, S., Zhou, T., Angélil, O., & Shiogama, H. (2017a). Increased chances of drought
596 in southeastern periphery of the Tibetan Plateau induced by anthropogenic
597 warming. Journal of Climate, 30(16), 6543-6560. https://doi.org/10.1175/JCLI-D-
598 16-0636.1

599 Ma, S., Zhou, T., Stone, D. A., Angélil, O., & Shiogama, H. (2017b). Attribution of the
600 July–August 2013 heat event in central and eastern China to anthropogenic
601 greenhouse gas emissions. Environmental Research Letters, 12(5), 054020. doi:
602 10.1088/1748-9326/aa69d2
603 Ma, S., Zhu, C., Liu, B., Zhou, T., Ding, Y., & Orsolini, Y. J. (2018). Polarized response
604 of East Asian winter temperature extremes in the era of Arctic warming. Journal
605 of Climate, 31(14), 5543-5557. https://doi.org/10.1175/JCLI-D-17-0463.1
606 Maher, N., Milinski, S., Suarez‐Gutierrez, L., Botzet, M., Dobrynin, M., Kornblueh,
607 L., ... & Marotzke, J. (2019). The Max Planck Institute Grand Ensemble:
608 enablingthe exploration of climate system variability. Journal of Advances in
609 Modeling Earth Systems, 11(7), 2050-2069.
610 https://doi.org/10.1029/2019MS001639
611 McCusker, K. E., Fyfe, J. C., & Sigmond, M. (2016). Twenty-five winters of
612 unexpected Eurasian cooling unlikely due to Arctic sea-ice loss. Nature
613 Geoscience, 9(11), 838-842. https://doi.org/10.1038/ngeo2820
614 Mori, M., Watanabe, M., Shiogama, H., Inoue, J., & Kimoto, M. (2014). Robust Arctic
615 sea-ice influence on the frequent Eurasian cold winters in past decades. Nature
616 Geoscience, 7(12), 869-873. https://doi.org/10.1038/ngeo2277
617 Norris, J., Chen, G., & Neelin, J. D. (2019). Thermodynamic versus dynamic controls
618 on extreme precipitation in a warming climate from the Community Earth System
619 Model Large Ensemble. Journal of Climate, 32(4), 1025-1045.
620 https://doi.org/10.1175/jcli-d-18-0302.1

621 Overland, J. E., Wood, K. R., & Wang, M. (2011). Warm Arctic—cold continents:
622 climate impacts of the newly open Arctic Sea. Polar Research, 30(1), 15787.
623 https://doi.org/10.3402/polar.v30i0.15787
624 Peings, Y., & Magnusdottir, G. (2014). Response of the wintertime Northern
625 Hemisphere atmospheric circulation to current and projected Arctic sea ice decline:
626 A numerical study with CAM5. Journal of Climate, 27(1), 244-264.
627 https://doi.org/10.1175/JCLI-D-13-00272.1
628 Qian, C., Wang, J., Dong, S., Yin, H., Burke, C., Ciavarella, A., ... & Tett, S. F. (2018).
629 Human Influence on the Record-breaking Cold Event in January of 2016 in
630 Eastern China. [in "Explaining Extreme Events of 2016 from a Climate
631 Perspective"]. Bulletin of the American Meteorological Society, 99(1), S118-S122.
632 https://doi.org/10.1175/BAMS-D-17-0095.1
633 Rahimzadeh, F., Asgari, A., & Fattahi, E. (2009). Variability of extreme temperature
634 and precipitation in Iran during recent decades. International Journal of
635 Climatology: A Journal of the Royal Meteorological Society, 29(3), 329-343.
636 https://doi.org/10.1002/joc.1739
637 Räisänen, J., & Ylhäisi, J. S. (2011). Cold months in a warming climate. Geophysical
638 Research Letters, 38(22). https://doi.org/10.1029/2011GL049758
639 Röthlisberger, M., & Papritz, L. (2023). A global quantification of the physical
640 processes leading to near - surface cold extremes. Geophysical Research
641 Letters, 50(5), e2022GL101670.

642 Sanderson, B. M., Xu, Y., Tebaldi, C., Wehner, M., O'Neill, B., Jahn, A., ... & Lamarque,
643 J. F. (2017). Community climate simulations to assess avoided impacts in 1.5 and
644 2 C futures. Earth System Dynamics, 8(3), 827-847. https://doi.org/10.5194/esd-
645 8-827-2017
646 Seneviratne, S. I., Corti, T., Davin, E. L., Hirschi, M., Jaeger, E. B., Lehner, I., ... &
647 Teuling, A. J. (2010). Investigating soil moisture–climate interactions in a
648 changing climate: A review. Earth-Science Reviews, 99(3-4), 125-161.
649 Shepherd, T. G. (2014). Atmospheric circulation as a source of uncertainty in climate
650 change projections. Nature Geoscience, 7(10), 703-708.
651 https://doi.org/10.1038/ngeo2253
652 Sheridan, S. C., & Allen, M. J. (2015). Changes in the frequency and intensity of
653 extreme temperature events and human health concerns. Current Climate Change
654 Reports, 1(3), 155-162. https://doi.org/10.1007/s40641-015-0017-3
655 Smoliak, B. V., Wallace, J. M., Lin, P., & Fu, Q. (2015). Dynamical adjustment of the
656 Northern Hemisphere surface air temperature field: Methodology and application
657 to observations. Journal of Climate, 28(4), 1613-1629.
658 https://doi.org/10.1175/JCLI-D-14-00111.1
659 Steponkus, P. L. (1979). Cold hardiness and freezing injury of agronomic crops.
660 Advances in Agronomy, 30, 51-98. https://doi.org/10.1016/S0065-
661 2113(08)60703-8

662 Sun, L., Perlwitz, J., & Hoerling, M. (2016). What caused the recent “Warm Arctic,
663 Cold Continents” trend pattern in winter temperatures?. Geophysical Research
664 Letters, 43(10), 5345-5352. https://doi.org/10.1002/2016GL069024
665 Sun, Y., Zhang, X., Zwiers, F. W., Song, L., Wan, H., Hu, T., ... & Ren, G. (2014). Rapid
666 increase in the risk of extreme summer heat in Eastern China. Nature Climate
667 Change, 4(12), 1082-1085. https://doi.org/10.1038/nclimate2410
668 Thompson, D. W., & Wallace, J. M. (1998). The Arctic Oscillation signature in the
669 wintertime geopotential height and temperature fields. Geophysical research
670 letters, 25(9), 1297-1300. https://doi.org/10.1029/98GL00950
671 Thompson, D. W., Wallace, J. M., Jones, P. D., & Kennedy, J. J. (2009). Identifying
672 signatures of natural climate variability in time series of global-mean surface
673 temperature: Methodology and insights. Journal of Climate, 22(22), 6120-6141.
674 https://doi.org/10.1175/2009JCLI3089.1
675 Thornton, H. E., Hoskins, B. J., & Scaife, A. A. (2016). The role of temperature in the
676 variability and extremes of electricity and gas demand in Great Britain.
677 Environmental Research Letters, 11(11), 114015. doi: 10.1088/1748-
678 9326/11/11/114015
679 Trenary, L., DelSole, T., Tippett, M. K., & Doty B. (2016). Extreme Eastern US Winter
680 of 2015 Not Symptomatic of Climate Change [in “Explaining Extreme Events of
681 2016 from a Climate Perspective”]. Bulletin of the American Meteorological
682 Society, 97(12), S31-S35. doi: 10.1175/BAMS-D-16-0156.1

683 Wallace, J. M., Fu, Q., Smoliak, B. V., Lin, P., & Johanson, C. M. (2012). Simulated
684 versus observed patterns of warming over the extratropical Northern Hemisphere
685 continents during the cold season. Proceedings of the National Academy of
686 Sciences, 109(36), 14337-14342. https://doi.org/10.1073/pnas.1204875109
687 Walsh, J. E. (2014). Intensified warming of the Arctic: Causes and impacts on middle
688 latitudes. Global and Planetary Change, 117, 52-63.
689 Wang, C., Yao, Y., Wang, H., Sun, X., & Zheng, J. (2021). The 2020 summer floods and
690 2020/21 winter extreme cold surges in China and the 2020 typhoon season in the
691 western North Pacific. Advances in Atmospheric Sciences. 38, 896 – 904.
692 https://doi.org/10.1007/s00376-021-1094-y
693 Wang, L., Deng, A., & Huang, R. (2019). Wintertime internal climate variability over
694 Eurasia in the CESM large ensemble. Climate dynamics, 52(11), 6735-6748.
695 https://doi.org/10.1007/s00382-018-4542-3
696 Westra, S., Fowler, H. J., Evans, J. P., Alexander, L. V., Berg, P., Johnson, F., ... &
697 Roberts, N. (2014). Future changes to the intensity and frequency of short‐
698 duration extreme rainfall. Reviews of Geophysics, 52(3), 522-555.
699 https://doi.org/10.1002/2014RG000464
700 Xu, M., Xu, H., & Ma, J. (2016). Responses of the East Asian winter monsoon to global
701 warming in CMIP5 models. International Journal of Climatology, 36(5), 2139-
702 2155. https://doi.org/10.1002/joc.4480

703 Yamaguchi, K., & Noda, A. (2006). Global warming patterns over the North Pacific:
704 ENSO versus AO. Journal of the Meteorological Society of Japan. Ser. II, 84(1),
705 221-241. https://doi.org/10.2151/jmsj.84.221
706 Zhang, W., Zhou, T., Zou, L., Zhang, L., & Chen, X. (2018). Reduced exposure to
707 extreme precipitation from 0.5C less warming in global land monsoon regions.
708 Nature Communications, 9(1), 3153. https://doi.org/10.1038/s41467- 018-05633-
709 3
710 Zhou, T., Zhang, W., Zhang, L., Clark, R., Qian, C., Zhang, Q., ... & Zhang, X. (2022).
711 2021: A Year of Unprecedented Climate Extremes in Eastern Asia, North America,
712 and Europe. Advances in Atmospheric Sciences. 39, 1598 – 1607.
713 https://doi.org/10.1007/s00376-022-2063-9
714 Zhou, W., Li, C., & Wang, X. (2007). Possible connection between Pacific oceanic
715 interdecadal pathway and East Asian winter monsoon. Geophysical Research
716 Letters, 34(1). https://doi.org/10.1029/2006GL027809
717

718 **Table 1** The list of observed cold months in period of 1962-2011 boreal winter.

Time (Year Month)	Total(℃)	Dynamic(℃)	Thermodynamic(℃)	Dynamic ratio (%)
196402	-5.63	-3.30	-2.33	58.6
196902	-5.02	-2.77	-2.25	55.1
197701	-4.51	-2.52	-1.98	56.0
196802	-4.35	-1.16	-3.19	26.6
196712	-4.01	-2.02	-2.00	50.3
201101	-3.47	-3.81	0.34	109.9
197202	-3.39	-0.45	-2.93	13.4
196612	-3.30	-2.55	-0.75	77.1

719

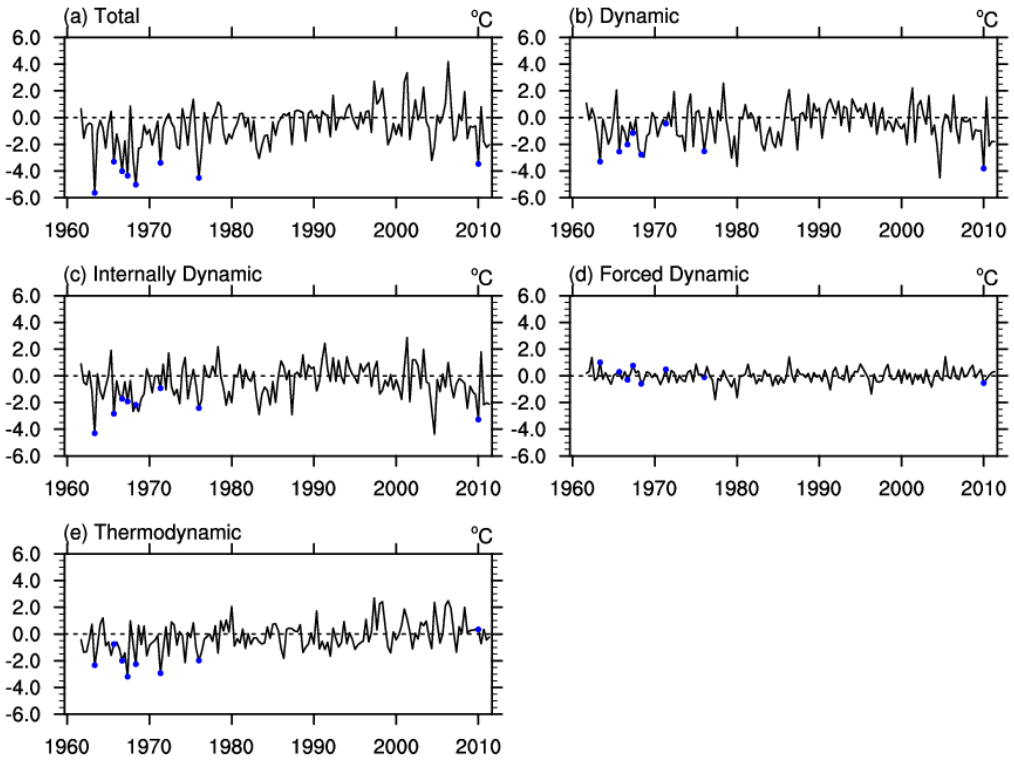
(a) Total
°C
(b) Dynamic
°C
(c) Internally Dynamic
°C
(d) Forced Dynamic
°C
(e) Thermodynamic
°C
6.0
4.0
2.0
0.0
-2.0
-4.0
-6.0
1960
1970
1980
1990
2000
2010

720

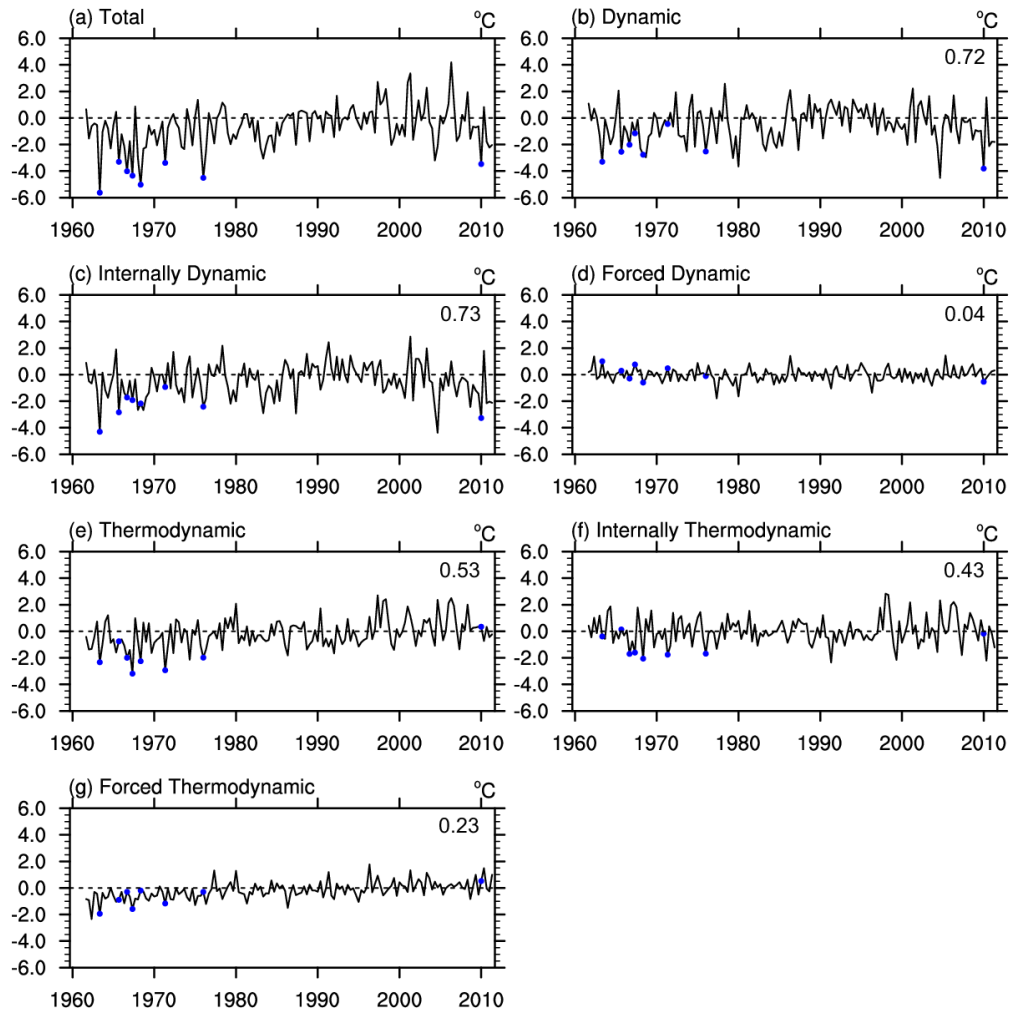
(a) Total
°C
(b) Dynamic
°C
0.72
(c) Internally Dynamic
°C
0.73
(d) Forced Dynamic
°C
0.04
(e) Thermodynamic
°C
0.53
(f) Internally Thermodynamic
°C
0.43
(g) Forced Thermodynamic
°C
0.23
6.0
4.0
2.0
0.0
-2.0
-4.0
-6.0
1960
1970
1980
1990
2000
2010

721

Figure 1 Time series decomposition of winter monthly surface air temperature (SAT) anomalies averaged over East Asia (20°N-55°N and from 105°E-130°E) from the observation into internal, forced, dynamic and thermodynamic components: (a) total, (b) dynamic, (c) internally dynamic, (d) forced dynamic and (e) thermodynamic components. The blue dots represent the cold months in the period of 1962-2011 boreal winter. The numbers in the upper right corner of subplots (b) to (g) represent the correlation coefficient between each component of SAT anomaly and the original SAT anomaly shows in subplot (a).

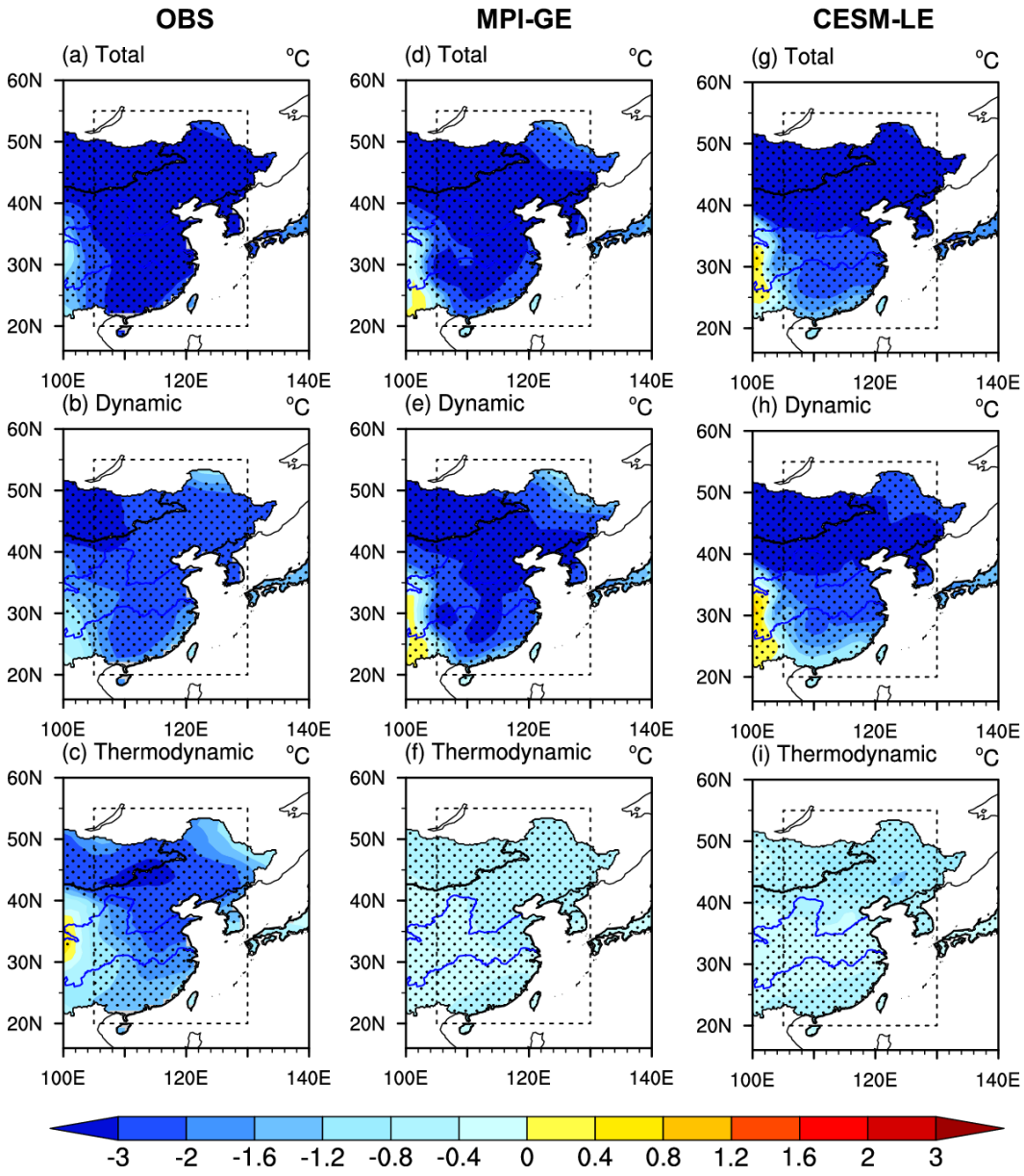

731

732 **Figure 2** The composites of the cold-month SAT anomaly (relative to the 1986-2005

733 boreal winter climatology) in the observation during the period of 1962-2011 boreal

734 winter: (a) total, (b) dynamically-induced and (c) thermodynamically-induced. The

735 subplots (d)-(f) and (g)-(i) correspond to subplots (a)-(c), but for the results in the MPI-

736 GE and the CESM-LE, respectively. The dotted areas are statistically significant at the

737 5% level according to Student's t test. The cold months are defined as months in which

738 SAT is lower than the statistical 5th percentile of all the monthly SAT samples during

739 1962-2011 boreal winter.

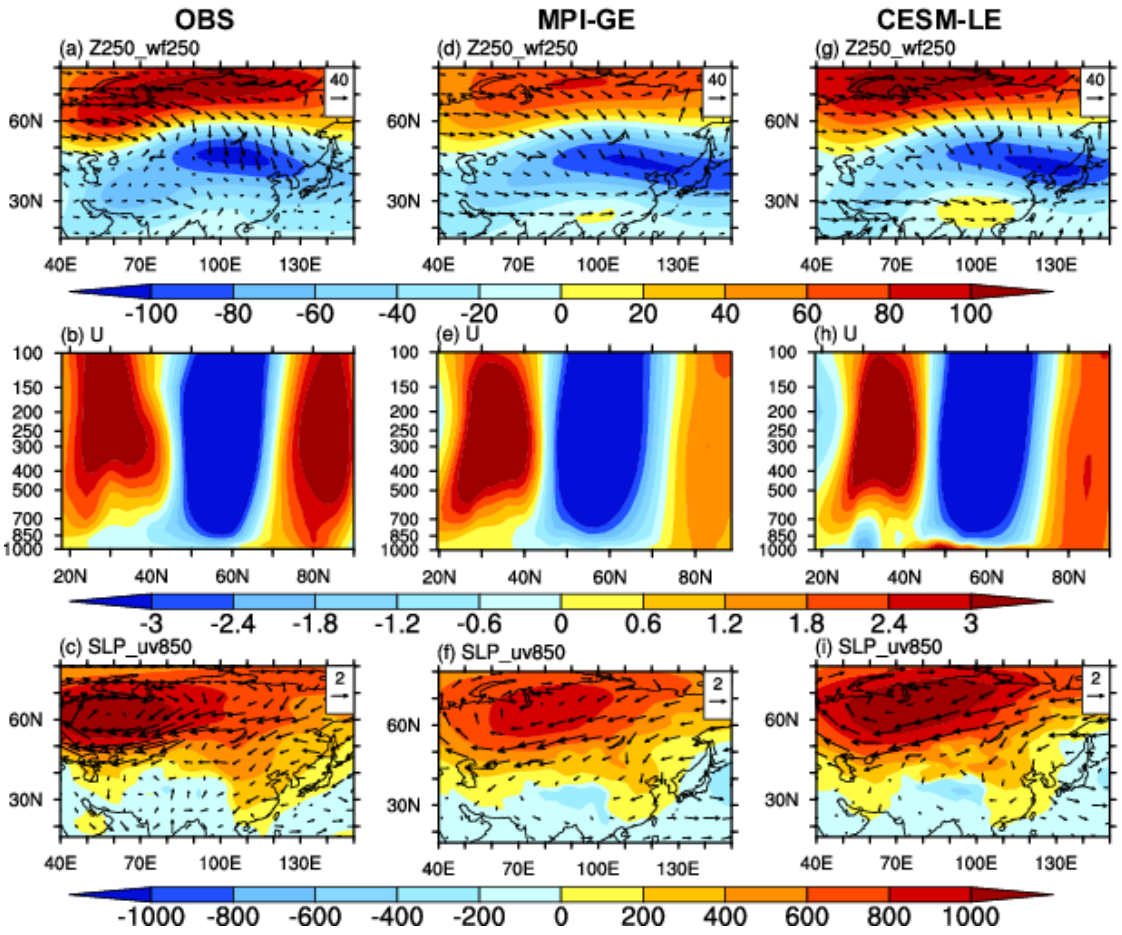
OBS
MPI-GE
CESM-LE
(a) Z250_wf250
(d) Z250_wf250
(g) Z250_wf250
40
60N
30N
40E
70E
100E
130E
-100 -80 -60 -40 -20 0 20 40 60 80 100
(b) U
(e) U
(h) U
100
150
200
250
300
400
500
700
850
1000
20N
40N
60N
80N
-3 -2.4 -1.8 -1.2 -0.6 0 0.6 1.2 1.8 2.4 3
(c) SLP_uv850
(f) SLP_uv850
(i) SLP_uv850
2
-1000 -800 -600 -400 -200 0 200 400 600 800 1000

740

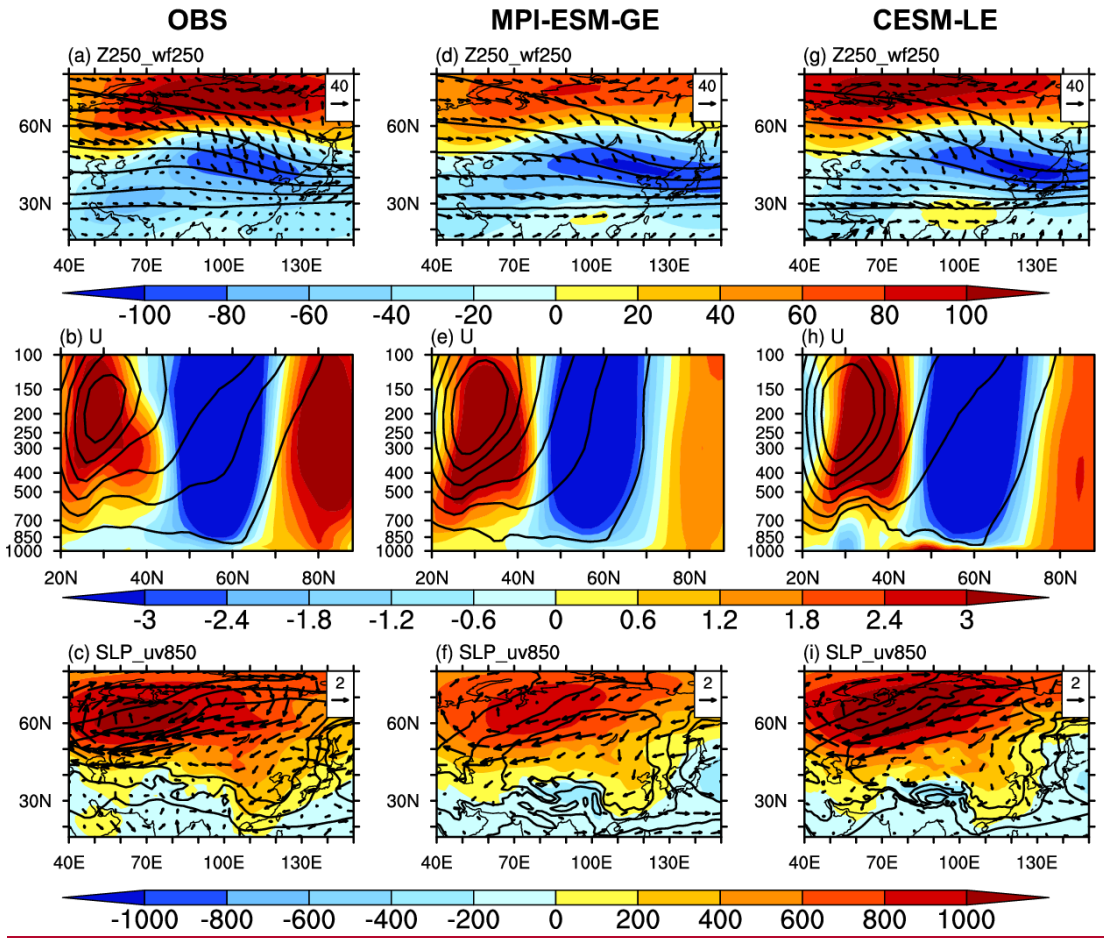

741

742 **Figure 3** Observed composite circulation anomalies (relative to the 1986-2005 boreal
743 winter climatology) for East Asian cold extremes during the period of 1962-2011 boreal
744 winter: (a) Geopotential height (shading; unit: m) and horizontal components of the
745 wave activity flux ($m^2 s^{-2}$) at 250-hPa. (b) Zonal mean zonal wind over the vertical cross
746 section (zonally averaged over 70-120°E; unit: m s^{-1};). (c) ~~sea~~Sea level pressure
747 (shading; unit: Pa) and horizontal wind at 850-hPa (m s^{-1}). The contours in subplots (a)-
748 (c) represent the 1986-2005 boreal winter climatology of geopotential height at 250-
749 hPa, zonal mean zonal wind over the vertical cross section, and sea level pressure,
750 respectively. Subplots (d)-(f) and (g)-(i) correspond to subplots (a)-(c), but for the
751 results in the MPI-GE and the CESM-LE, respectively.

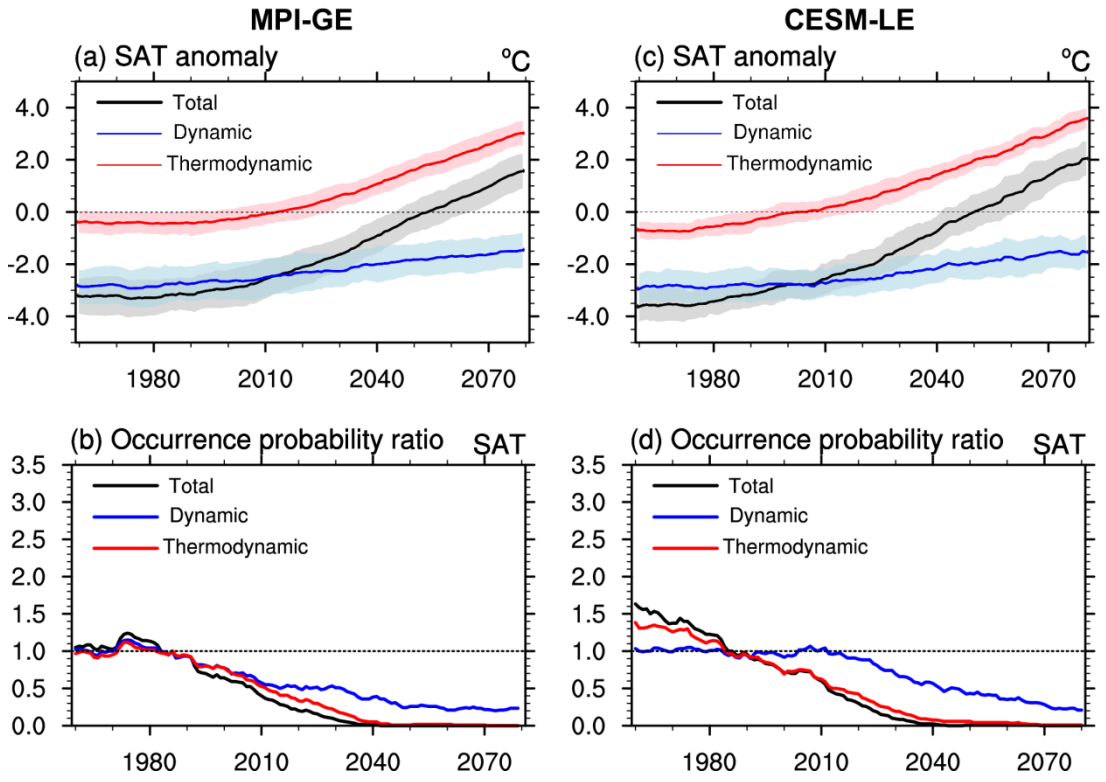

Figure 4 (a) Time series of the 20-yr running averaged cold-month SAT anomaly (black) and its dynamically-induced (blue) and thermodynamically-induced (red) components over East Asia relative to the 1986-2005 boreal winter climatology in the MPI-GE. The shading shows the range of two standard deviations among the model members. (b) Time series of the occurrence probability ratio of the present-day East Asian cold extremes in the MPI-GE: both dynamic and thermodynamic components change (black), only dynamic component changes (blue) and only thermodynamic component change (red). Subplots (c) and (d) correspond to subplots (a) and (b), but for the results in the CESM-LE. cold months are defined as the months in which the regional mean SAT is lower than the statistical 5th percentile of the climatological monthly SAT series during DJF in a certain time slice.

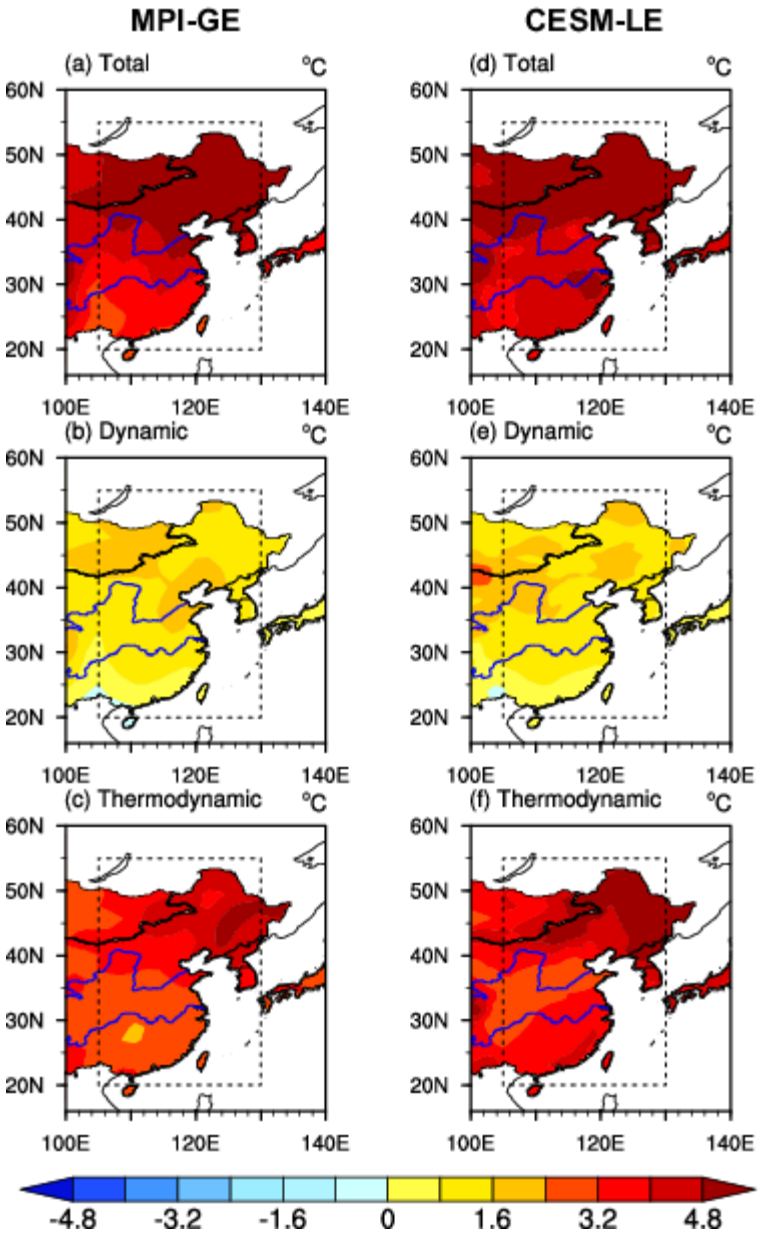

764

765 **Figure 5** Changes in East Asian cold-month SAT in the MPI-GE in 2079-2098 boreal

766 winter relative to 1986-2005 boreal winter: (a) Total, (b) dynamic component and (c)

767 thermodynamic component. Subplots (d)-(f) correspond to subplots (a)-(c), but for the

768 results in the CESM-LE.

769

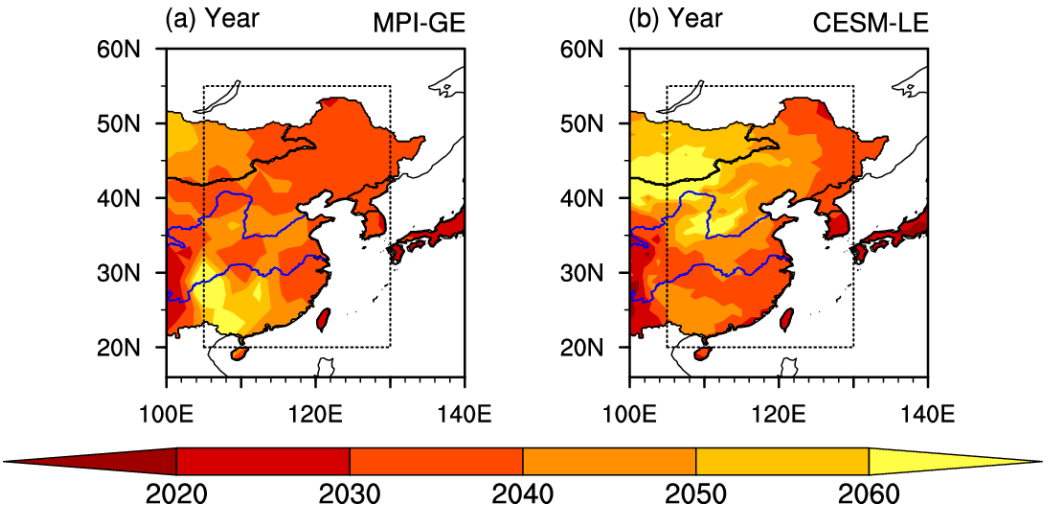

Figure 6 The year when the occurrence probability ratio of the present-day (1986-2005 boreal winter) East Asian cold extremes decreases to 0.05 in (a) The MPI-GE and (b) the CESM-LE.

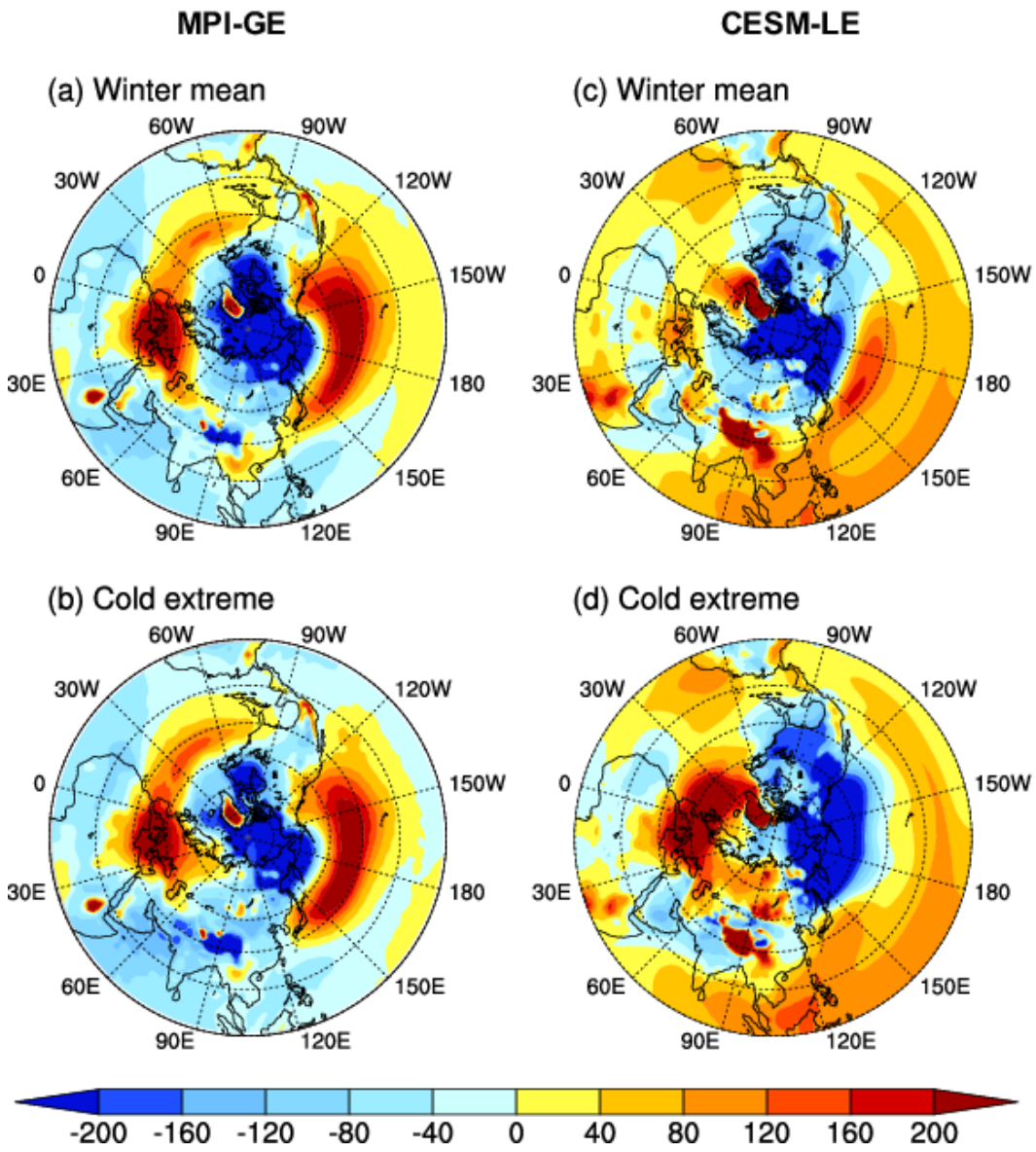

774

775 **Figure 7** Changes in SLP for (a) total winter months and (b) cold months in 2079-2098

776 boreal winter relative to 1986-2005 boreal winter in the MPI-GE. Subplots (c) and (d)

777 correspond to subplots (a) and (b), but for the results in the CESM-LE.

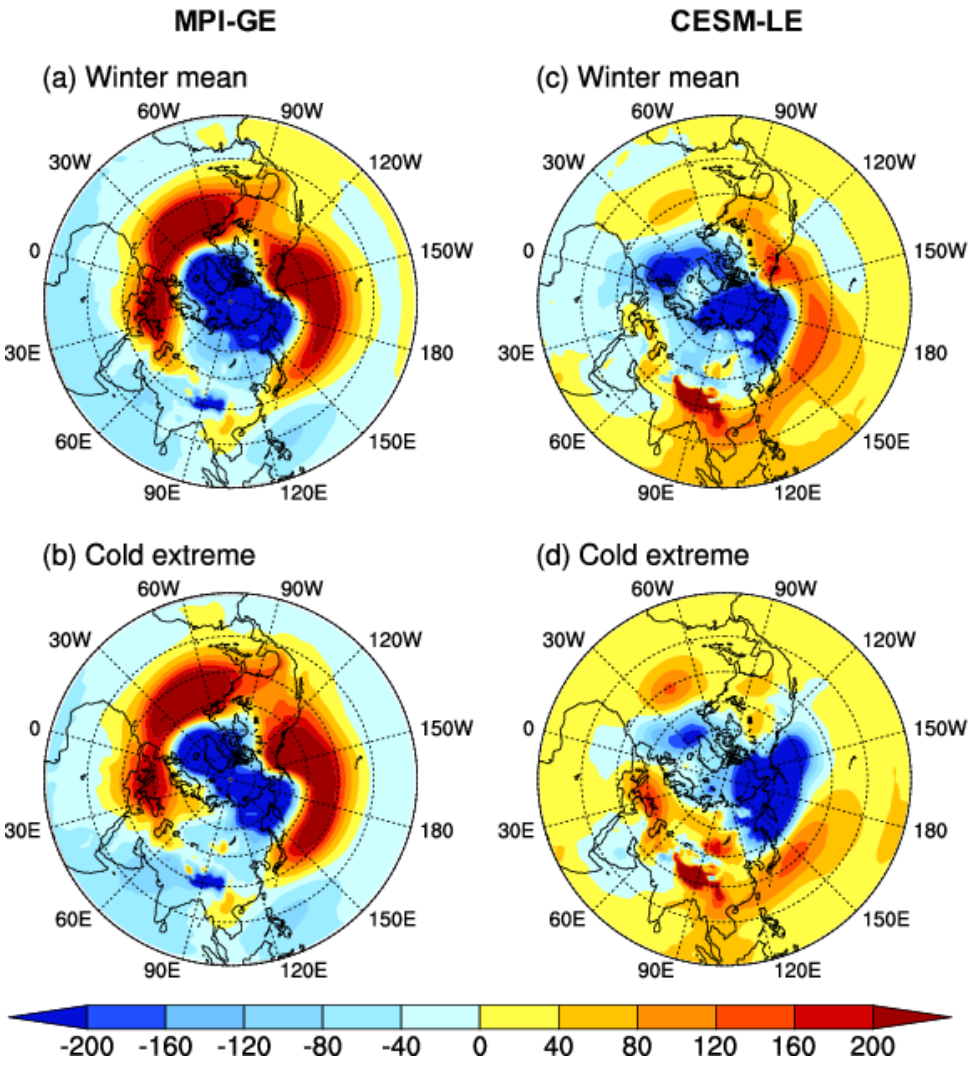

778

779 **Figure 8** Changes in the dynamic component of SLP for (a) total winter months and (b)

780 cold months in 2079-2098 boreal winter relative to 1986-2005 boreal winter in the MPI-

781 GE. Subplots (c) and (d) correspond to subplots (a) and (b), but for the results in the

782 CESM-LE.

783